CWP-667

Moveout inversion of wide-azimuth P-wave data for tilted TI media

Xiaoxiang Wang & Ilya Tsvankin
Center for Wave Phenomena, Geophysics Department, Colorado School of Mines, Golden, Colorado 80401

ABSTRACT
TTI (transversely isotropic with a tilted symmetry axis) models have been widely used for velocity analysis and imaging in many exploration areas, such as the Canadian Foothills and the Gulf of Mexico. In a previous publication, we discussed 2D stacking-velocity inversion for the interval parameters of TTI media composed of homogeneous layers separated by plane interfaces. Here, this 2D algorithm is extended to 3D wide-azimuth data by including P-wave NMO ellipses and two horizontal slowness components (time slopes) in the objective function. If the symmetry axis is perpendicular to the bottom of each layer, it is possible to estimate the interval symmetry-direction velocity V_{P0}, anisotropy parameter δ, and the reflector orientation using only one borehole constraint – the reflector depth. The algorithm can tolerate small (1/10 of the dip) deviation of the symmetry axis from the reflector normal. However, as is the case for the 2D problem, the parameter ϵ can seldom be constrained without using nonhyperbolic moveout inversion. If the symmetry axis deviates from the reflector normal but is confined to the dip plane, stable parameter estimation requires a relationship between the tilt and dip in each layer. When the tilt represents a free parameter, the input data have to be supplemented by wide-azimuth VSP traveltimes with the offset reaching at least 1/4 of the maximum reflector depth. Moreover, the additional angle coverage provided by VSP data may help resolve the parameter ϵ in the upper part of the model.

Key words: transverse isotropy, tilted symmetry axis, TTI, P-wave, wide-azimuth, azimuthal anisotropy, NMO ellipse, borehole, VSP

1 INTRODUCTION

Transversely isotropic media with a tilted symmetry axis (TTI) provide marked improvements in prestack imaging of P-wave data (Charles *et al.*, 2008; Huang *et al.*, 2008; Neal *et al.*, 2009). Allowing for the symmetry-axis tilt results in more plausible velocity models for sedimentary formations in complex geological settings (Vestrum *et al.*, 1999; Behera & Tsvankin, 2009; Bakulin *et al.*, 2009).

P-wave velocities and traveltimes in TTI media can be expressed through the symmetry-direction velocity V_{P0} and Thomsen (1986) anisotropy parameters ϵ and δ defined with respect to the symmetry axis. The symmetry-axis orientation is defined by the tilt angle ν with the vertical and the azimuth β. Although many migration algorithms have been extended to TTI media, accurate estimation of the interval anisotropy parameters and the symmetry-axis orientation remains a difficult problem.

For example, Grechka *et al.* (2001) discuss 2D inversion of P-wave normal-moveout (NMO) velocities and zero-offset traveltimes for the parameters of a dipping TTI layer with the symmetry axis perpendicular to the bedding. Their algorithm is based on several *a priori* assumptions about the model and requires reflection data from a horizontal interface beneath the TTI layer.

A review of several other parameter-estimation algorithms for TTI media (e.g., Grechka *et al.*, 2002a) can be found in our previous publication (Wang & Tsvankin, 2010, hereafter referred to as Paper I), where we develop a 2D inversion methodology for a stack of homogeneous

TTI layers separated by plane dipping interfaces. P-wave NMO velocities, reflection slopes, and zero-offset traveltimes are supplemented with reflector depths measured in a borehole, as well as with check-shot and near-offset VSP traveltimes. Even for a single TTI layer, the medium parameters cannot be resolved without constraining the tilt of the symmetry axis. Therefore, in Paper I the symmetry axis is assumed to be orthogonal to the layer's bottom, which is typical for dipping shale layers (Isaac & Lawton, 1999; Vestrum *et al.*, 1999; Charles *et al.*, 2008). As a result, the 2D algorithm produces stable estimates of the interval parameters V_{P0} and δ provided the range of dips does not exceed 30°.

Here, we present a 3D extension of the inversion algorithm from Paper I by including the NMO ellipses and two horizontal slownesses (reflection time slopes) in the objective function. Wide-azimuth data provide additional information for estimating the interval Thomsen parameters, which helps relax the constraints on model geometry and increase the stability of the inversion. First, we discuss parameter estimation for models with the symmetry axis orthogonal to reflectors. Then we extend the method to models with arbitrary tilt and show that stable inversion requires the addition of VSP data. Synthetic tests on noise-contaminated data help evaluate the accuracy and stability of estimating the interval TTI parameters for different types of input data.

2 3D INPUT DATA VECTOR

As in Paper I, we consider a stack of homogeneous TTI layers separated by plane, dipping, non-intersecting boundaries (Figure 1). However, the dip planes of model interfaces no longer have to be aligned. From 3D multi-azimuth P-wave data recorded at a common midpoint (CMP) with the coordinates $\mathbf{Y} = [\mathrm{Y}_1, \mathrm{Y}_2]$, we obtain the zero-offset reflection traveltimes $t_0(\mathbf{Y}, n)$ for all reflectors, the corresponding NMO velocities $V_{\rm nmo}(\alpha)$ (α is the azimuth), and the time slopes $\mathbf{p}(\mathbf{Y}, n) = [p_1(\mathbf{Y}, n), p_2(\mathbf{Y}, n)]$, where p_1 and p_2 are the horizontal slowness components of the zero-offset ray. The azimuthally-dependent NMO velocity is described by an elliptical function in the horizontal plane (Grechka & Tsvankin, 1998):

$$V_{\rm nmo}^{-2}(\alpha) = W_{11}\cos^2\alpha + 2W_{12}\sin\alpha\cos\alpha + W_{22}\sin^2\alpha\,, \quad (1)$$

where $\mathbf{W}$ is a symmetric matrix,

$$W_{ij} = \tau_0 \frac{\partial^2 \tau}{\partial x_i \partial x_j}\bigg|_{\mathbf{x}=\mathbf{Y}}, \quad (i,j=1,2)\,. \quad (2)$$

Here $\tau(x_1, x_2)$ is the one-way traveltime from the zero-offset reflection point to the location $\mathbf{x}\{x_1, x_2\}$ at the surface and τ_0 is the one-way zero-offset traveltime. The matrices $\mathbf{W}(\mathbf{Y}, n)$ can be obtained from azimuthal velocity analysis of reflection data based on the hyperbolic moveout equation parameterized by the NMO ellipse (Grechka & Tsvankin, 1999).

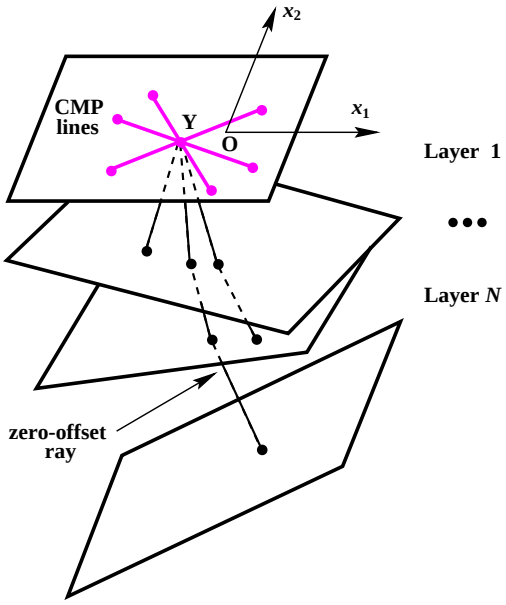

Figure 1. Zero-offset rays and a multiazimuth CMP gather for a model composed of a stack of TTI layers separated by plane dipping interfaces (after Grechka *et al.*, 2002b).

Grechka & Tsvankin (2002) devise a Dix-type averaging procedure to model the effective NMO ellipse for heterogeneous anisotropic media. They show that the exact NMO ellipse can be obtained by averaging the intersections of the interval NMO-velocity surfaces with the layer boundaries. All information for computing the NMO ellipse of a given reflection event is contained in the results of tracing just one (zero-offset) ray.

Because each layer is homogeneous with plane boundaries (Figure 1), it is sufficient to acquire the input data in a single multiazimuth CMP gather (Grechka *et al.*, 2002b). The reflector depths $z_{\rm b}(n)$ are assumed to be measured in a borehole, which may be placed away from the CMP location (the subscript "b" denotes borehole data). Therefore, the vector of input data for 3D inversion is as follows:

$$\mathbf{d} = \{t_0(n), p_1(n), p_2(n), W_{11}(n), W_{12}(n), W_{22}(n), z_{\rm b}(n)\} \quad (n = 1, 2, \ldots, N)\,, \quad (3)$$

where all components are the effective quantities for the n-th reflector.

3 SYMMETRY AXIS ORTHOGONAL TO THE REFLECTOR

It is common to put constraints on the symmetry-axis orientation using *a priori* information (Charles *et al.*, 2008; Huang *et al.*, 2008; Bakulin *et al.*, 2009). If TI layers were rotated by tectonic processes after sedimen-

tation, the symmetry axis typically remains perpendicular to the layering, which means that its tilt ν and azimuth β coincide with the dip ϕ and azimuth ψ of the reflector, respectively. The relative simplicity of this model significantly improves the stability of parameter estimation.

3.1 Inversion for a single TTI layer

First, we consider a homogeneous TTI layer with the symmetry axis orthogonal to its bottom. The dip plane of the reflector represents a vertical symmetry plane for the whole model, and therefore, includes one of the axes of the NMO ellipse. Thus, the orientation of the NMO ellipse yields the reflector azimuth ψ which coincides with the symmetry-axis azimuth β.

The semiaxis of the NMO ellipse in the dip plane is obtained from the isotropic cosine-of-dip relationship (Tsvankin, 2005):

$$V_{\rm nmo}^{(1)}(\phi) = \frac{V_{\rm nmo}(0)}{\cos\phi}\,, \tag{4}$$

where $V_{\rm nmo}(0) = V_{P0}\sqrt{1+2\delta}$ is the NMO velocity from a horizontal interface beneath a VTI medium (i.e., the symmetry axis is rotated along with the reflector). Alternatively, the dip component of the NMO velocity can be represented using the ray parameter $p = \sqrt{p_1^2 + p_2^2}$:

$$V_{\rm nmo}^{(1)}(p) = \frac{V_{\rm nmo}(0)}{\sqrt{1 - p^2 V_{P0}^2}}\,, \tag{5}$$

where $p = \sin\phi/V_{P0}$ because the phase-velocity vector of the zero-offset ray (and the ray itself) is parallel to the symmetry axis. The strike component $V_{\rm nmo}^{(2)}$ of the NMO velocity is given by (Grechka & Tsvankin, 2000):

$$V_{\rm nmo}^{(2)} = V_{\rm nmo}(0) = V_{P0}\sqrt{1+2\delta}\,. \tag{6}$$

Therefore, by combining the two semiaxes of the NMO ellipse (equations 5 and 6) and using the measured time slope p, we can find the symmetry-direction velocity V_{P0}. Then the dip $\phi = \nu$ is obtained from equation 4, and the anisotropy parameter δ from equation 6. Depth information for a single layer is not needed because the reflector depth z below the CMP location can be computed from the zero-offset traveltime t_0:

$$z = \frac{V_{P0}\, t_0}{2\cos\phi}\,. \tag{7}$$

However, P-wave hyperbolic moveout in this model is independent from the anisotropy parameter ϵ. In summary, the geometry and the parameters V_{P0} and δ of a single TTI layer can be resolved without using any borehole information.

3.2 Inversion for layered TTI media

Here, we present a 3D extension of the 2D stacking-velocity inversion algorithm from Paper I ("stacking-velocity tomography") to layered TTI media. If the symmetry axis in each layer is perpendicular to its bottom ($\nu^{(n)} = \phi^{(n)}$ and $\beta^{(n)} = \psi^{(n)}$), the model vector is

$$\mathbf{m} = \{V_{P0}^{(n)}, \epsilon^{(n)}, \delta^{(n)}, \phi^{(n)}, \psi^{(n)}\}\,, \quad (n = 1, 2, \ldots, N)\,. \tag{8}$$

First, we assume the depths $z_{\rm b}(n)$ to be known from borehole measurements; later on, we discuss the inversion without using the depth constraint.

3.2.1 Inversion methodology

As in Paper I, we specify the trial set $\mathbf{m}$ of the interval parameters (equation 8) and trace zero-offset rays through the model with the geometry partially fixed by the known reflector depths. The ray-tracing results yield the zero-offset traveltimes $t_0^{\rm calc}(n)$, the horizontal slowness components $p_1^{\rm calc}(n)$ and $p_2^{\rm calc}(n)$, and the Dix-type averaging procedure produces the effective NMO ellipses $\mathbf{W}^{\rm calc}(n)$. The NMO velocity $V_{\rm nmo}^{\rm calc}(n,\alpha)$ for any azimuth α can be computed from equation 1.

The vector $\mathbf{m}$ (equation 8) is estimated by minimizing the following objective function (based on L^2-norm) for all N reflectors simultaneously:

$$\mathcal{F}(\mathbf{m}) \equiv \sum_{n=1}^{N} \left\{ \frac{\left\|p_1^{\rm calc}(n) - p_1(n)\right\|^2}{\sigma^2[p_1(n)]} + \frac{\left\|p_2^{\rm calc}(n) - p_2(n)\right\|^2}{\sigma^2[p_2(n)]} + \frac{\left\|t_0^{\rm calc}(n) - t_0(n)\right\|^2}{\sigma^2[t_0(n)]} + \frac{\left\|V_{\rm nmo}^{\rm calc}(n,\alpha) - V_{\rm nmo}(n,\alpha)\right\|^2}{\sigma^2[V_{\rm nmo}(n,\alpha)]} \right\}, \tag{9}$$

where σ^2 represents the variance of each measurement, and the azimuth α varies from 0° to 180°. For 2D models, the objective function also includes check-shot traveltimes, and reflector dips are assumed to be known. Here, wide-azimuth data provide additional information that replaces those borehole constraints.

In a single TTI layer, the parameter ϵ cannot be found from conventional-spread P-wave moveout. However, as discussed in Paper I, $\mathbf{p}(n)$, $t_0(n)$, and $\mathbf{W}(n)$ for layered TTI models are influenced by the values of $\epsilon^{(n)}$ in the overburden (except for models with parallel interfaces). Therefore, the interval parameter ϵ is estimated along with the other unknowns, although it is not expected to be well-constrained.

3.2.2 Synthetic examples

As in Paper I, the algorithm was tested for a suite of layered TTI models ($0 \le \epsilon \le 0.5$ and $-0.2 \le \delta \le 0.3$) with reflector dips ranging from 0° to 60°. Table 2 shows the inversion results for a three-layer medium with relatively close azimuths of the interfaces (Table 1 and Figure 2). The results of a test for another three-layer medium with a wide range of interface azimuths but identical dips (Table 1 and Figure 3) are listed in Table 3. The inversion is performed for 200 realizations of

	Layer 1	Layer 2	Layer 3
V_{P0} (km/s)	1.5	2.0	2.5
ϵ	0.10	0.20	0.25
δ	-0.10	0.10	0.12

Table 1. Interval parameters of a three-layer TTI model.

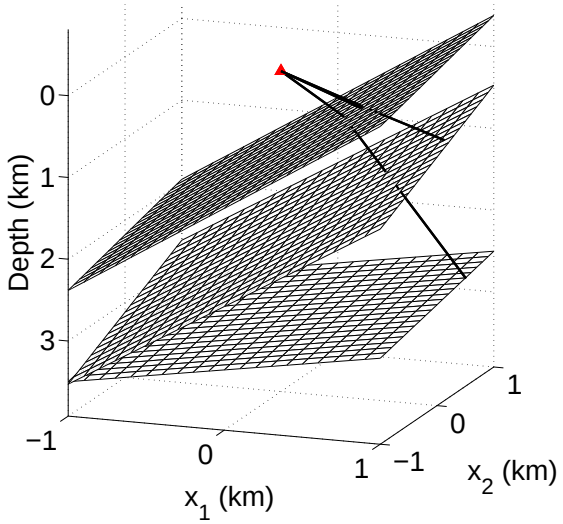

Figure 2. Zero-offset P-wave rays in a three-layer TTI model with the interval parameters listed in Table 1. The input data are computed by anisotropic ray tracing. The symmetry axis in each layer is perpendicular to its bottom. The dips and azimuths are $\phi^{(1)} = \phi^{(2)} = 50°$, $\phi^{(3)} = 20°$, $\psi^{(1)} = 10°$, $\psi^{(2)} = 20°$, and $\psi^{(3)} = 30°$. The reflector depths below the CMP (located at the origin of the coordinate system) are $z_b(1) = 1$ km, $z_b(2) = 2$ km, and $z_b(3) = 3$ km.

noise-contaminated input data using the measurement values as the variances σ^2 in equation 9.

For both models, the interval parameters V_{P0} and δ and the reflector dips and azimuths are recovered with sufficiently high accuracy. As expected, the standard deviations are higher in the third (deepest) layer (about 5% for V_{P0} and 0.06 for δ), primarily due to the smaller contribution of the deeper layers to the effective reflection traveltimes. However, in contrast to layer-stripping techniques, our tomography-style algorithm possesses the advantage of mitigating error accumulation with depth. An important factor that influences the inversion accuracy is the layer thickness; the thickness-to-depth ratio below the CMP location should reach at least 0.25 to ensure stable interval estimates. As expected, the standard deviations of the parameter ϵ are much larger than those of δ, although ϵ-estimates are not substantially biased.

For plausible ranges of ϵ and δ ($|\epsilon| \le 0.5$; $|\delta| \le 0.3$), the errors in the interval parameters V_{P0}, δ, ϕ, and ψ remain small if the symmetry axis deviates from the reflector normal in the dip plane by less than one tenth of the dip value ($\phi/10$; i.e., $\beta = \psi$, but $\nu \neq \phi$). For example, we used the tilts $\nu^{(n)} = 9\,\phi^{(n)}/10$ ($n = 1, 2, 3$) for the second model (Table 1 and Figure 3) to generate the input data and applied our algorithm assuming that $\nu^{(n)} = \phi^{(n)}$ (Table 4). The slight deviation of the symmetry axis from the reflector normal causes a mild bias in the estimates, but the standard deviations are mostly controlled by the noise level, which is the same as in the previous tests.

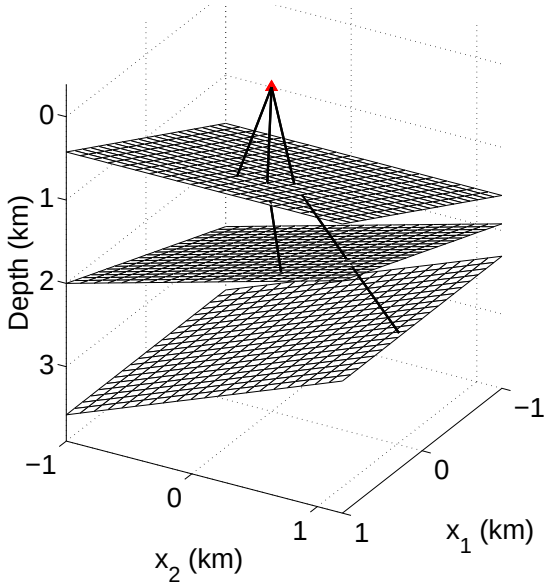

Figure 3. Zero-offset P-wave rays in a three-layer TTI model with the interval parameters listed in Table 1. The symmetry axis in each layer is perpendicular to its bottom. The dips and azimuths are $\phi^{(1)} = \phi^{(2)} = \phi^{(3)} = 30°$, $\psi^{(1)} = 0°$, $\psi^{(2)} = 45°$, and $\psi^{(3)} = 90°$. The reflector depths below the CMP are $z_b(1) = 1$ km, $z_b(2) = 2$ km, and $z_b(3) = 3$ km.

If the reflector depths are also unknown, the trade-off between $z(n)$ and other parameters increases errors in the inversion results. For example, we performed the inversion for the previous model (Table 1 and Figure 3) without using depth information for the same level of noise in the input data. The standard deviations of V_{P0} and δ in the third layer increase to 7% and 0.09, respectively. The mean values of V_{P0} (2.61 km/s) and δ (0.08) are also strongly biased. The mean value of $z(3)$ (actual quantity is 3 km) is 3.04 km with the standard deviation 0.12 km.

4 SYMMETRY AXIS DEVIATING FROM REFLECTOR NORMAL

The assumption of the symmetry axis being perpendicular to the reflector is too restrictive when tectonic processes and sedimentation occur together (Bakulin *et al.*, 2009). Also, for stress-induced anisotropy in sediments

	V_{P0} (km/s)		δ		ϵ		ϕ (°)		ψ (°)	
	mean	sd (%)	mean	sd	mean	sd	mean	sd	mean	sd
Layer 1	1.50	1	-0.10	0.01	0.21	0.22	50.0	0.2	10.0	0.1
Layer 2	2.00	3	0.10	0.03	0.25	0.11	50.0	0.4	19.9	0.3
Layer 3	2.49	5	0.12	0.06	0.25	0.23	20.2	2.2	30.1	1.9

Table 2. Inversion results for the three-layer TTI model from Table 1 and Figure 2. The input data are distorted by Gaussian noise with the standard deviations equal to 1% for $p_1(n)$, $p_2(n)$, and $t_0(n)$, and 2% for the NMO velocities. The mean values and standard deviations of the inverted parameters are denoted by "mean" and "sd," respectively.

	V_{P0} (km/s)		δ		ϵ		ϕ (°)		ψ (°)	
	mean	sd (%)	mean	sd	mean	sd	mean	sd	mean	sd
Layer 1	1.50	1	-0.10	0.01	0.10	0.04	30.0	0.3	0.0	0.1
Layer 2	2.00	2	0.10	0.03	0.20	0.07	30.0	0.3	45.1	1.4
Layer 3	2.51	5	0.12	0.06	0.26	0.23	30.0	0.5	90.1	2.0

Table 3. Inversion results for the three-layer TTI model from Table 1 and Figure 3. The noise level in the input data is the same as in Table 2.

near salt bodies, the symmetry is largely controlled by the principal stress direction which is not necessarily aligned with the normal to the bedding (Bakulin *et al.*, 2009).

To account for the deviation of the symmetry axis from the reflector normal, the tilt ν can be expressed as a function of the dip ϕ using geologic data. For example, the simultaneous influence of tectonic forces and sedimentation typically makes ν smaller than ϕ (e.g., $\nu = \phi/2$ or $\nu = 3\,\phi/4$). In the next test, we use the three-layer model with the interval parameters listed in Table 1 and the model geometry shown in Figure 2, but with $\nu \neq \phi$. The symmetry axis in each layer is confined to the dip plane (i.e., $\beta^{(n)} = \psi^{(n)}$, $n = 1, 2, 3$) with the tilt $\nu^{(n)} = \phi^{(n)}/2$. The known relationship between ν and ϕ is sufficient for the algorithm to produce stable estimates of the interval parameters V_{P0} and δ and the reflector orientation (Table 5).

4.1 Tilt as an unknown parameter

Here, we relax the assumption that the tilt ν represents a known function of the dip ϕ. It is still assumed that the symmetry-axis azimuth β in each layer coincides with the dip-plane azimuth ψ, but the parameter ν has to be found from the inversion. Thus, the model vector includes one more unknown:

$$\mathbf{m} = \{V_{P0}^{(n)}, \epsilon^{(n)}, \delta^{(n)}, \nu^{(n)}, \phi^{(n)}, \psi^{(n)}\}\,, \quad (n = 1, 2, \ldots, N)\,. \tag{10}$$

Making ν a free parameter significantly increases the nonuniqueness of the inversion. For 2D models, simultaneous estimation of V_{P0}, ϵ, δ, and ν proves to be ambiguous, even if the reflector depths and dips are measured in a borehole. Our tests indicate that 3D wide-azimuth data supplemented by the known reflector depths still cannot be used to resolve the tilt along with the other TTI parameters. Therefore, we propose to add wide-azimuth walkaway VSP (vertical seismic profiling) traveltimes $t_{\rm VSP}$ to the input data:

$$\mathbf{d} = \{t_0(n), p_1(n), p_2(n), W_{11}(n), W_{12}(n), W_{22}(n), z_{\rm b}(n), t_{\rm VSP}\}\,. \tag{11}$$

We employ an array of sources at the surface and one VSP receiver per layer located close to the layer's bottom. Similar to the zero-offset reflected rays, we trace VSP rays in a trial model and compute the difference between the modeled and observed traveltimes. Then, the objective function takes the form

$$\mathcal{F}(\mathbf{m}) \equiv \sum_{n=1}^{N} \left\{ \frac{\left\|p_1^{\rm calc}(n) - p_1(n)\right\|^2}{\sigma^2[p_1(n)]} + \frac{\left\|p_2^{\rm calc}(n) - p_2(n)\right\|^2}{\sigma^2[p_2(n)]} + \frac{\left\|t_0^{\rm calc}(n) - t_0(n)\right\|^2}{\sigma^2[t_0(n)]} + \frac{\left\|t_{\rm VSP}^{\rm calc} - t_{\rm VSP}\right\|^2}{\sigma^2[t_{\rm VSP}]} + \frac{\left\|V_{\rm nmo}^{\rm calc}(n,\alpha) - V_{\rm nmo}(n,\alpha)\right\|^2}{\sigma^2[V_{\rm nmo}(n,\alpha)]} \right\}. \tag{12}$$

4.1.1 Synthetic examples

Numerical testing shows that it is sufficient to add one check-shot source and several VSP sources located around the borehole with the offset exceeding 1/4 of the largest reflector depth. To achieve full azimuthal coverage, eight VSP sources are placed along a circle with a

	V_{P0} (km/s)		δ		ϕ (°)		ψ (°)	
	mean	sd (%)	mean	sd	mean	sd	mean	sd
Layer 1	1.50	1	-0.10	0.01	29.8	0.3	0.0	0.0
Layer 2	1.99	2	0.09	0.03	30.3	0.3	44.3	1.4
Layer 3	2.50	5	0.10	0.06	30.1	0.5	89.5	2.0

Table 4. Inversion results for the three-layer TTI model from Table 1 with the model geometry shown in Figure 3. The symmetry axis in each layer is confined in the dip plane, but is no longer perpendicular to the reflector ($\nu^{(1)} = \nu^{(2)} = \nu^{(3)} = 27°$). The noise level is the same as in the previous tests.

	V_{P0} (km/s)		δ		ν (°)		ψ (°)	
	mean	sd (%)	mean	sd	mean	sd	mean	sd
Layer 1	1.50	1	-0.10	0.01	25.0	0.2	10.0	0.0
Layer 2	2.01	4	0.10	0.06	25.0	0.4	20.0	0.5
Layer 3	2.50	4	0.12	0.04	10.0	0.6	30.0	0.8

Table 5. Inversion results for the three-layer TTI model from Table 1 with the model geometry shown in Figure 2. The tilt of the symmetry axis in each layer is equal to one-half of the reflector dip. The noise level is the same as in the previous tests.

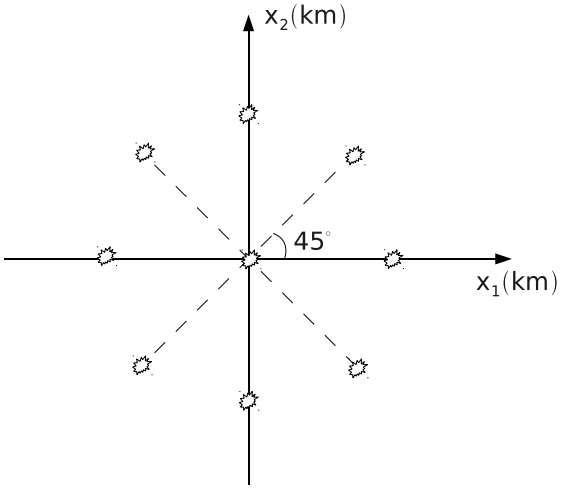

Figure 4. Distribution of VSP sources at the surface. The check-shot source is located close to the borehole ($x_1 = 0.01$, $x_2 = 0$). The VSP lines are separated by 45°, and the offset of each VSP source is 1 km.

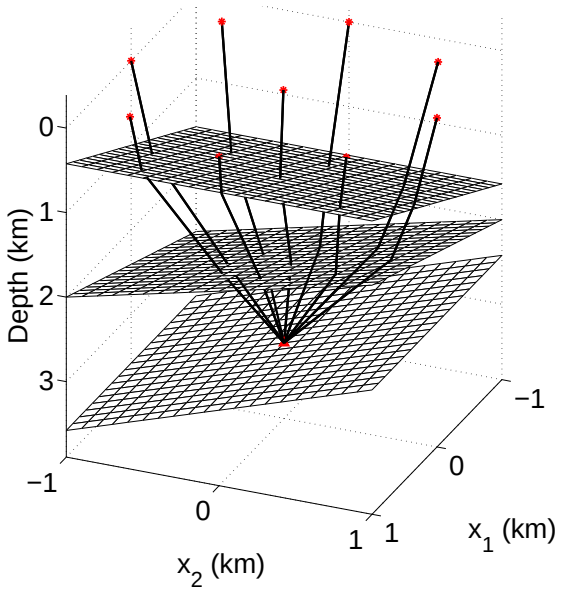

Figure 5. VSP rays for the receiver located at the bottom of a three-layer TTI model with the interval parameters listed in Table 1. The symmetry axis in each layer is confined in the dip plane. The tilts, dips, and azimuths are $\nu^{(1)} = \nu^{(2)} = \nu^{(3)} = 20°$, $\phi^{(1)} = \phi^{(2)} = \phi^{(3)} = 30°$, $\psi^{(1)} = 0°$, $\psi^{(2)} = 45°$, and $\psi^{(3)} = 90°$. The vertical borehole is below the coordinate origin, and the reflector depths at the borehole location are $z_b(1) = 1$ km, $z_b(2) = 2$ km, and $z_b(3) = 3$ km.

45° increment in azimuth (Figure 4). With this distribution of the VSP sources, we compute the input data for a three-layer model (Table 1 and Figure 5) using anisotropic ray tracing. The inversion results for 100 realizations of noise-contaminated data are listed in Table 6. We also test another model with larger tilt angles $\nu^{(1)} = \nu^{(2)} = \nu^{(3)} = 40°$ (Table 7).

Despite the additional constraints provided by VSP data, the standard deviations in the tilt increase rapidly with depth because the inversion for ν is still ill-conditioned. However, the interval parameters V_{P0} and δ and the reflector orientation can be recovered with sufficient accuracy. Also, the VSP data help constrain the parameter ϵ in the top two layers, while estimation of ϵ in the bottom layer is ambiguous because of the reduced

	V_{P0} (km/s)		δ		ϵ		ν (°)		ϕ (°)		ψ (°)	
	mean	sd (%)	mean	sd	mean	sd	mean	sd	mean	sd	mean	sd
Layer 1	1.50	1	-0.10	0.01	0.10	0.02	20.9	2.8	30.0	0.5	0.0	0.4
Layer 2	2.00	1	0.09	0.03	0.21	0.06	20.3	5.0	30.0	0.6	45.3	1.0
Layer 3	2.48	2	0.13	0.06	0.24	0.12	23.9	10.1	30.1	0.8	90.0	1.1

Table 6. Inversion results for the three-layer TTI model from Table 1 using reflection and VSP data (Figure 5). The positions of the check-shot and VSP sources are shown in Figure 4. The tilts are $\nu^{(1)} = \nu^{(2)} = \nu^{(3)} = 20°$. The input data are distorted by Gaussian noise with the standard deviations equal to 1% for $p_1(n)$, $p_2(n)$, $t_0(n)$, and $t^{\rm calc}_{\rm VSP}$, and 2% for the NMO velocities.

	V_{P0} (km/s)		δ		ϵ		ν (°)		ϕ (°)		ψ (°)	
	mean	sd (%)	mean	sd	mean	sd	mean	sd	mean	sd	mean	sd
Layer 1	1.50	1	-0.10	0.01	0.10	0.01	40.0	0.9	30.0	0.5	0.1	0.5
Layer 2	2.00	1	0.10	0.03	0.21	0.05	40.4	6.5	30.0	0.6	45.1	0.8
Layer 3	2.50	3	0.12	0.06	0.31	0.11	39.0	12.5	29.9	0.8	90.0	1.1

Table 7. Inversion results for the three-layer TTI model from Table 1 using reflection and VSP data (Figure 5). The positions of the check-shot and VSP sources are shown in Figure 4. The tilts are $\nu^{(1)} = \nu^{(2)} = \nu^{(3)} = 40°$. The noise level is the same as in Table 6.

angle coverage of the VSP rays at depth. To resolve the parameter ϵ in piecewise homogeneous TTI models, it is necessary to use long-offset VSP or reflection data.

It should be mentioned that the deviation of the symmetry axis from the reflector normal reduces the stability of parameter estimation. When the difference between ν and ϕ is large, small errors in the input data are significantly amplified by the inversion algorithm. Therefore, the tilt should be confined to the range $\phi/2 \le \nu \le 3\phi/2$, which is typical for most TTI formations.

5 DISCUSSION AND CONCLUSIONS

The tilt of the symmetry axis in TI media makes the medium azimuthally anisotropic, and wide-azimuth P-wave data provide valuable constraints on the TTI parameters. If the symmetry axis is perpendicular to the reflector, the P-wave NMO ellipse is sufficient for estimating the parameters V_{P0} and δ of a single dipping TTI layer. Conventional-spread P-wave data also yield the depth and orientation of the reflector, but the parameter ϵ remains unconstrained without using long-offset moveout.

For homogeneous TTI layers separated by plane dipping interfaces, the input data include the effective NMO ellipses, zero-offset traveltimes, and reflection slopes supplemented by the reflector depths measured in a borehole. The interval parameters are estimated by a 3D tomography-style algorithm that represents an extension of the 2D method introduced in Paper I. As long as the symmetry axis in each layer is kept orthogonal to its bottom, the interval parameters V_{P0} and δ and the reflector dips ϕ and azimuths ψ are well-resolved. If the magnitude of anisotropy is not uncommonly large ($|\epsilon| \le 0.5$; $|\delta| \le 0.3$), small deviations of the symmetry axis from the reflector normal ($\pm\phi/10$) do not distort the inversion results. Inversion without depth information produces parameter estimates with larger bias and standard deviation.

If the symmetry axis is not perpendicular to the reflector but the tilt represents a known function of the reflector dip ϕ, the 3D inversion algorithm can still resolve V_{P0}, δ, and the reflector orientation. We also examined the possibility of estimating the tilt from the data under the assumption that the symmetry axis is confined to the dip plane of the reflector. Numerical testing demonstrates that stable inversion requires additional input data, such as check-shot and walkaway VSP traveltimes. VSP data should have full azimuthal coverage and the distance between the VSP sources and the borehole has to reach 1/4 of the largest reflector depth. Another essential requirement is for the tilt to fall into the range $\phi/2 \le \nu \le 3\phi/2$. Depending on the offset range of VSP data, it may be possible to constrain the parameter ϵ in the shallow part of the section.

Velocity variations on the scale of conventional spread-length may cause errors in the estimated parameters. Our aim, however, is to design an efficient algorithm for building an initial TTI model using wide-azimuth P-wave data at several borehole locations. An accurate initial model may help ensure the convergence of velocity-analysis algorithms that operate in the migrated domain (e.g., reflection tomography).

6 ACKNOWLEDGMENTS

We are grateful to Vladimir Grechka (Shell) and Andres Pech (IPN, Mexico) for making available their codes. We also thank Andrey Bakulin (WesternGeco), Paul Fowler (WesternGeco), and Ken Larner (CWP) for numerous helpful suggestions. This work was supported by the Consortium Project on Seismic Inverse Methods for Complex Structures at CWP.

References

Bakulin, A., Woodward, M., Nichols, D., Osypov, K., & Zdraveva, O. 2009. Building TTI depth models using anisotropic tomography with well information. *79th Annual International Meeting, SEG, Expanded Abstracts*, 4029–4033.

Behera, L., & Tsvankin, I. 2009. Migration velocity analysis for tilted TI media. *Geophysical Prospecting*, **57**, 13–26.

Charles, S., Mitchell, D. R., Holt, R. A., Lin, J., & Mathewson, J. 2008. Data-driven tomographic velocity analysis in tilted transversely isotropic media: A 3D case history from the Canadian Foothills. *Geophysics*, **73**, VE261–VE268.

Grechka, V., & Tsvankin, I. 1998. 3D description of normal moveout in anisotropic inhomogeneous media. *Geophysics*, **63**, 1079–1092.

Grechka, V., & Tsvankin, I. 1999. 3D moveout inversion in azimuthally anisotropic media with lateral velocity variation: theory and a case study. *Geophysics*, **64**, 1202–1218.

Grechka, V., & Tsvankin, I. 2000. Inversion of azimuthally dependent NMO velocity in transversely isotropic media with a tilted axis of symmetry. *Geophysics*, **65**, 232–246.

Grechka, V., & Tsvankin, I. 2002. NMO-velocity surfaces and Dix-type formulas in anisotropic heterogeneous media. *Geophysics*, **67**, 939–951.

Grechka, V., Pech, A., Tsvankin, I., & Han, B. 2001. Velocity analysis for tilted transversely isotropic media: A physical-modeling example. *Geophysics*, **66**, 904–910.

Grechka, V., Pech, A., & Tsvankin, I. 2002a. Multicomponent stacking-velocity tomography for transversely isotropic media. *Geophysics*, **67**, 1564–1574.

Grechka, V., Pech, A., & Tsvankin, I. 2002b. P-wave stacking-velocity tomography for VTI media. *Geophysical Prospecting*, **50**, 151–168.

Huang, T., Xu, S., Wang, J., Ionescu, G., & Richardson, M. 2008. The benefit of TTI tomography for dual azimuth data in Gulf of Mexico. *78th Annual International Meeting, SEG, Expanded Abstracts*, 222–226.

Isaac, J. H., & Lawton, D. C. 1999. Image mispositioning due to dipping TI media: A physical seismic modeling study. *Geophysics*, **64**, 1230–1238.

Neal, Scott L., Hill, N. Ross, & Wang, Yue. 2009. Anisotropic velocity modeling and prestack Gaussian-beam depth migration with applications in the deepwater Gulf of Mexico. *The Leading Edge*, **28**, 1110–1119.

Thomsen, L. 1986. Weak elastic anisotropy. *Geophysics*, **51**, 1954–1966.

Tsvankin, I. 2005. *Seismic signatures and analysis of reflection data in anisotropic media, 2nd edition*. Elsevier Science Publ. Co., Inc.

Vestrum, R. W., Lawton, D. C., & Schmid, R. 1999. Imaging structures below dipping TI media. *Geophysics*, **64**, 1239–1246.

Wang, X., & Tsvankin, I. 2010. Stacking-velocity inversion with borehole constraints for tilted TI media. *Geophysics (accepted for publication)*.